

Extracting Primordial Density Fluctuations

Eric Gawiser and Joseph Silk

The combination of detections of anisotropy in cosmic microwave background radiation and observations of the large-scale distribution of galaxies probes the primordial density fluctuations of the universe on spatial scales varying by three orders of magnitude. These data are found to be inconsistent with the predictions of several popular cosmological models. Agreement between the data and the cold + hot dark matter model, however, suggests that a significant fraction of the matter in the universe may consist of massive neutrinos.

Shortly after the Big Bang, the universe was smooth to a precision of one part in 10^5 . We can measure this smoothness in cosmic microwave background (CMB) radiation—photons that provide us with a record of conditions in the early universe, because they were last scattered about 300,000 years after the Big Bang. To a remarkably precise degree, the early universe was characterized by isotropic homogeneous expansion. However, temperature fluctuations have been measured in the CMB (1), and complex structure surrounds us. There is a simple connection: The seeds of large-scale structure were infinitesimal density perturbations that grew through gravitational instability into massive structures such as galaxies and galaxy clusters.

One can search for the primordial seeds of large-scale structure with two complementary techniques. CMB fluctuations probe the density fluctuations in the early universe on comoving scales greater than ~ 100 Mpc. The gravity field of these density fluctuations also generates fluctuations in the distribution of luminous galaxies, as well as deviations, known as peculiar velocities, from the Hubble flow of universal expansion. Optical redshift surveys of galaxies can now examine a range of scales up to ~ 100 Mpc that overlaps with the range probed by fluctuations in the CMB.

The expected rate of growth of density fluctuations depends on the precise cosmology adopted (2). One can therefore use the comparison between CMB anisotropy and fluctuations in galaxy distribution to discriminate among rival cosmological models. Scott *et al.* (3) have illustrated this comparison. Several similar analyses (4–7) have been presented but have used only a portion

of the compilation of observations we present here.

Structure Formation Models

We examined 10 models of structure formation (Table 1), which represent the range of cosmological parameters that are currently considered viable (8). Each model gives transfer functions that predict how a primordial power spectrum of infinitesimal density perturbations in the early universe develops into CMB anisotropies and inhomogeneities in the distribution of galaxies. A cosmological model whose predictions agree with both types of observations provides a consistent picture of structure formation on scales ranging from galaxy clusters to the present horizon size. The cosmological parameter $\Omega = \Omega_m + \Omega_\Lambda$ gives the ratio of the energy density of the universe to the critical density that is necessary to stop its expansion. Critical density is $\rho_c = 3H_0^2/8\pi G$ for a Hubble constant of $H_0 = 100 h \text{ km}^{-1} \text{ s}^{-1} \text{ Mpc}^{-1}$ (G is the gravitational constant). The portion of this critical energy density contained in matter is $\Omega_m = \Omega_c + \Omega_\nu + \Omega_b$, which is the sum of the contributions from cold dark matter (CDM) (Ω_c), hot dark matter (HDM) in the form of massive neutrinos (Ω_ν), and baryonic matter (Ω_b). $\Omega_\Lambda = \Lambda/3H_0^2$ is the fraction of

the critical energy density contained in a smoothly distributed vacuum energy referred to as a cosmological constant, Λ . The age of the universe in each model is determined by the values of h , Ω_m , and Ω_Λ ; a universe with critical matter density has an age of $6.5 h^{-1} \text{ Gyr}$ ($\text{Gyr} = 10^9 \text{ years}$) (9).

Each model has a primordial power spectrum of density perturbations given by $P_p(k) = Ak^n$, for each wave number k , where A is the square of a free normalization parameter and n is the scalar spectral index (10). Scale invariance (11) corresponds to $n = 1$ for adiabatic (constant entropy) initial density perturbations and $n = -3$ for isocurvature (constant potential) initial density perturbations. Instead of normalizing to the Cosmic Background Explorer Satellite (COBE) result alone (12), we found the best-fit normalization of each model (Table 2) using the entire data compilation. Our rationale is that COBE is just one subset of the available data, albeit with small error bars, and is in fact the data most likely to be affected by a possible contribution of gravitational waves to CMB anisotropies. These gravitational waves from inflation would have a significant impact only on large angular scales and are not traced by the large-scale structure observations. Normalizing to all of the data made our results less sensitive to the possible contribution of gravitational waves.

The first seven models (Table 1) are based on the standard cold dark matter (SCDM) model (13) and assume that the initial density perturbations in the universe were adiabatic, as is predicted by the inflationary universe paradigm. The tilted CDM (TCDM) and cold + hot dark matter (CHDM) models are both motivated by changing the shape of the matter power spectrum of SCDM to eliminate its problem of excess power on small scales relative to large scales (7, 14). The CHDM model has one family of massive neutrinos that contributes 20% of the critical density (15). For the cosmological constant (Λ CDM) and open universe (OCDM) models, $\Omega_m = 0.5$, $h = 0.6$ roughly guarantees the right shape

Table 1. Values of cosmological parameters for our models. Parameters marked with an asterisk have been optimized (59).

Model	Ω	Ω_Λ	Ω_m	Ω_c	Ω_ν	Ω_b	h	n	Age (Gyr)
SCDM	1.0	0	1.0	0.95	0	0.05	0.5	1.0	13
TCDM	1.0	0	1.0	0.90	0	0.10*	0.5	0.8*	13
CHDM	1.0	0	1.0	0.70	0.2*	0.10*	0.5	1.0*	13
OCDM	0.5	0	0.5*	0.45	0	0.05*	0.6*	1.0*	12
Λ CDM	1.0	0.5	0.5*	0.45	0	0.05*	0.6*	1.0*	14
ϕ CDM	1.0	0	0.92	0.87	0	0.05	0.5	1.0	13
BCDM	1.0	0.88	0.12	0.08	0	0.04	0.8	1.6	15
ICDM	1.0	0.8	0.2	0.17	0	0.03	0.7	-1.8	15
PBH BDM	1.0	0.6	0.4	0	0	0.10	0.7	-2.0	13
Strings + Λ	1.0	0.7	0.3	0.25	0	0.05	0.5	~ 1	19

E. Gawiser is at the Department of Physics, University of California at Berkeley, Berkeley, CA 94720, USA. E-mail: gawiser@astron.berkeley.edu. J. Silk is at the Departments of Physics and Astronomy and the Center for Particle Astrophysics, University of California at Berkeley, Berkeley, CA 94720, USA.

of the matter power spectrum (5). We have optimized some parameters of these models: n and Ω_b for TCDM; Ω_m , Ω_b , n , and the number of massive neutrino families for CHDM; and Ω_m , Ω_b , h , and n for OCDM and Λ CDM (16). The ϕ CDM model (17) contains a vacuum energy contribution from a late-time scalar field with $\Omega_\phi = 0.08$. This energy behaves like matter today, but during matter-radiation equality and re-

combination it alters the shape of the matter and radiation power spectra from the otherwise similar SCDM model. The baryonic + cold dark matter (BCDM) model (18) contains nearly equal amounts of baryonic matter ($\Omega_b = 0.04$) and CDM ($\Omega_c = 0.08$). Its parameters have been tuned to produce a peak due to baryonic acoustic oscillations in the matter power spectrum at $k = 0.05 h \text{ Mpc}^{-1}$, where a similar peak is

seen in the three-dimensional power spectrum of rich Abell clusters (19) and the two-dimensional power spectrum of the Las Campanas Redshift Survey (20).

The isocurvature cold dark matter (ICDM) model (21, 22) has a non-Gaussian (χ^2) distribution of isocurvature density perturbations produced by a massive scalar field frozen during inflation. This causes early structure formation, in agreement with observations of galaxies at high redshift and the Lyman α forest (23). The primordial black hole baryonic dark matter (PBH BDM) model (24) has isocurvature perturbations but no CDM. The primordial black holes form from baryons in high-density regions of the early universe and thereafter behave like CDM. Only a tenth of the critical energy density remains outside the black holes to participate in nucleosynthesis. These black holes have the appropriate mass ($M \sim 1M_\odot$) to be the massive compact halo objects (MACHOS) that have been detected in our galaxy (25). Albrecht *et al.* found that topological defect models with critical matter density fail to agree with structure formation observations (26). In the strings + Λ model (27) that we examined, the nonzero cosmological constant causes a deviation from scaling and makes cosmic strings a viable model.

We used the CMBFAST code (28) to calculate the predicted radiation and matter power spectra for the SCDM, TCDM, CHDM, OCDM, Λ CDM, and BCDM models.

Constraints on Cosmological Parameters

The models we consider are all consistent with the constraints on the baryon density from Big Bang nucleosynthesis, $0.012 < \Omega_b h^2 < 0.026$, allowed by recent observations of primordial deuterium abundance (29). A Hubble constant of 65 ± 15 encompasses the range of systematic variations between different observational approaches (30). The age "crisis" has abated with a recent recalibration by Hipparcos of the distance to the oldest galactic globular clusters, leading to a new estimate of their age of 11.5 ± 1.3 Gyr (31). All of our models have an age of at least 13 Gyr except OCDM (12 Gyr). Other constraints, however, appear to limit the viability of our models. Observations of high-redshift damped Lyman α systems are a concern for the CHDM and TCDM models, which have little power at small scales (32). Bartelmann *et al.* (33) used numerical simulations to compare the observed abundance of arcs from strong lensing by galaxy clusters with the predictions of various models and concluded that only OCDM works, and

Table 2. Best-fit normalizations and biases. The normalization of each model is given by σ_8 or by the value of dT expected at $\ell = 10$, which can be compared to the COBE normalization of $dT = 27.9 \mu\text{K}$.

Model	$dT_{10} (\mu\text{K})$	σ_8	b_{clus}	b_{cfa}	b_{lcrs}	b_{apm}	b_{iras}
SCDM	25.4	1.08	2.12	0.83	0.72	0.89	0.57
TCDM	31.2	0.79	2.73	1.13	1.01	1.18	0.83
CHDM	27.1	0.75	2.52	1.11	1.01	1.13	0.78
OCDM	29.0	0.77	2.67	1.25	1.11	1.10	0.93
Λ CDM	26.8	1.00	2.14	0.91	0.82	0.87	0.68
ϕ CDM	27.6	0.74	3.12	1.35	1.20	1.31	0.98
BCDM	24.8	1.76	1.30	0.48	0.40	0.41	0.37
ICDM	28.2	0.83	2.95	1.25	1.12	1.02	0.97
PBH BDM	29.9	0.78	2.74	1.21	1.09	1.10	0.92
Strings + Λ	21.2	0.32	6.95	3.10	2.86	2.62	2.48

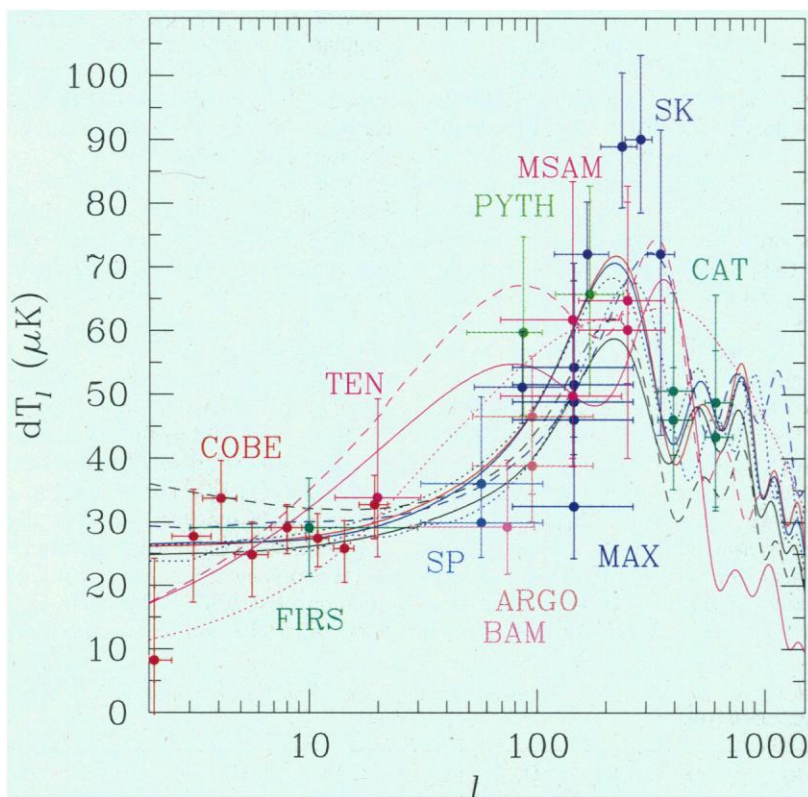


Fig. 1. Compilation of CMB anisotropy results, with horizontal error bars showing the full width at half maximum of each instrument's window function and vertical error bars showing the 68% confidence interval (61). The detections shown here are from COBE, FIRS, Tenerife, the South Pole, BAM, ARGO, Python, MAX, MSAM, SK, and CAT (62). Predictions for the models with their best-fit normalizations are plotted as $dT_\ell = [\ell(\ell + 1)C_\ell/2\pi]^{1/2}T_{\text{CMB}}$ for SCDM (solid black), TCDM (dashed black), CHDM (solid red), OCDM (dashed blue), Λ CDM (solid blue), ϕ CDM (dotted black), BCDM (dotted blue), ICDM (dashed magenta), PBH BDM (solid magenta), and strings + Λ (dotted magenta). The ICDM, PBH BDM, and strings + Λ models disagree with the slope implied by COBE, SP, and BAM, which prefers the adiabatic models. SK favors a high acoustic peak near $\ell = 250$ and has small error bars, making it a challenge for most models.

they found that critical density models seriously underpredict the number of arcs. Further support for low- Ω_m models comes from the cluster baryon fraction of $\Omega_m/\Omega_b \leq 23h^{3/2}$ (34). This favors the ratio of total matter to baryons in the low-matter-density models considered here and is inconsistent with SCDM and ϕ CDM. Observations of Type Ia supernovae at high red shift are progressing rapidly, and preliminary results argue in favor of a positive cosmological constant and strongly disfavor $\Omega_m = 1$ (35). The amount of vacuum energy is constrained to be $\Omega_\Lambda \leq 0.7$ by quasar lensing surveys (36). Direct observations of cosmological parameters favor the low- Ω_m models, but we found that the current discriminatory power of observations of structure formation outweighs that of direct parameter observations.

Comparison with Observations

Since the COBE differential microwave radiometer (DMR) detection of CMB anisotropy (1), there have been over 25 additional measurements of anisotropy on angular scales ranging from 7° to 0.3° . The models predict that the spherical harmonic decomposition of the pattern of CMB temperature (T_{CMB}) fluctuations on the sky will have Gaussian distributed coefficients $a_{\ell m}$ with zero mean and variance C_ℓ (ℓ is the multipole number of the spherical harmonic expansion of the pattern of CMB anisotropies on the sky). Each observation has a window function W_ℓ , which makes the total power measured sensitive to a range of angular scales given by $\theta \approx 180^\circ/\ell$:

$$\begin{aligned} \left(\frac{\Delta T}{T}\right)_{\text{rms}}^2 &= \frac{1}{4\pi} \sum_\ell (2\ell + 1) C_\ell W_\ell \\ &= \frac{1}{2} (dT/T_{\text{CMB}})^2 \sum_\ell \frac{2\ell + 1}{\ell(\ell + 1)} W_\ell \quad (1) \end{aligned}$$

where COBE found $dT = 27.9 \pm 2.5 \mu\text{K}$ and $T_{\text{CMB}} = 2.73 \text{ K}$ (37). This allows the observations of broad-band power to be reported as observations of dT ; and knowing the window function of an instrument, one can turn the predicted C_ℓ spectrum of a model into the corresponding prediction for dT at that angular scale (Fig. 1).

We translated these observations of the radiation power spectrum into estimates of the matter power spectrum on the same scales (38). The matter power spectrum is determined by the matter transfer function $T(k)$ and primordial power spectrum $P_p(k)$ of each model, with $P(k) = T^2(k)P_p(k)$. The matter transfer function describes the processing of initial density perturbations from the Big Bang during

the era of radiation domination; the earlier a spatial scale entered the horizon, the more its power was dissipated by radiation (and in the CHDM model, by relativistic neutrinos as well). If the baryon fraction is large, the same acoustic oscillations of the photon-baryon fluid that give rise to peaks in the radiation power spectrum are visible in the matter power spectrum; otherwise, the baryons fall into the potential wells of the dark matter. Once matter domination and recombination arrive, $P(k)$ maintains its shape and grows as $(1 + z)^{-2}$ (z is the redshift of a given epoch; $z = 0$ today). Thus, determining $P(k)$ today allows us to extract the power spectrum of primordial density fluctuations that existed when the universe was over a thousand times smaller.

Our compilation of observations of fluctuations in the large-scale distribution of gal-

axies and galaxy clusters (Fig. 2A) includes the determination of σ_8 , the rms density variation in spheres of radius $8 h^{-1} \text{ Mpc}$, based on the abundance of rich galaxy clusters (39). Another measurement of σ_8 is based on the evolution of the abundance of rich clusters from red shift 0.5 until now (40). The predicted value of σ_8 is given by an integral over the matter power spectrum, using a spherical top-hat window function of radius $R = 8 h^{-1} \text{ Mpc}$ (41)

$$\sigma_R^2 = \frac{1}{2\pi^2} \int dk k^2 P(k) \frac{9}{(kR)^6} (\sin kR - kR \cos kR)^2 \quad (2)$$

which allows observations of σ_8 to determine the amplitude of $P(k)$ on scales $k \approx 0.2 h \text{ Mpc}^{-1}$. Another measurement of the amplitude of the power spectrum comes from ob-

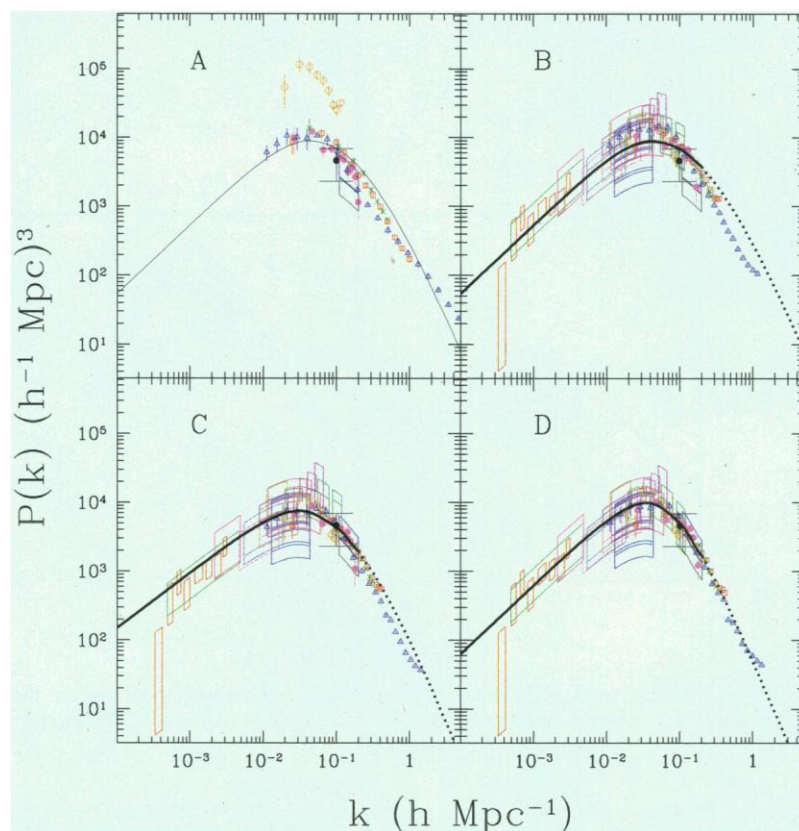


Fig. 2. (A) Compilation of large-scale structure observations, with $P(k)$ for SCDM (solid curve) shown for reference. No corrections for bias, redshift distortions, or nonlinear evolution have been made. k is the wave number in comoving units of $h \text{ Mpc}^{-1}$. The black and blue boxes are measurements of σ_8 from the present-day number abundance of rich clusters and its evolution, respectively (39, 40), and the black point with error bars is from peculiar velocities (42). $\Omega_m = 1$ is assumed (63). Uncorrected power spectra are shown for the APM galaxy survey (blue triangles), Las Campanas (red squares), IRAS (filled pink circles), APM clusters (orange circles), and SSRS2 + CfA2 (green crosses) (44, 43). (B) The SCDM model with its best-fit normalization compared to the large-scale structure data with its best-fit biases after model-dependent corrections for redshift distortions and nonlinear evolution (64). Beyond $k = 0.2 h \text{ Mpc}^{-1}$, the predicted matter power spectrum curve is dotted to indicate uncertainty in the data corrections. We plot each CMB anisotropy detection as a box, where the width of the box represents the range of k to which that experiment is most sensitive, and the height shows the 68% confidence interval (65). (C) The TCDM model. (D) CHDM, our best-fit model. Note the agreement even on nonlinear scales.

servations of peculiar velocities of galaxies (42).

Our data compilation includes power spectra from four redshift surveys: the Las Campanas Redshift Survey (LCRS), the combined Infrared Astronomical Satellite (IRAS) 1.2 Jy and QDOT samples (1 Jy = 10^{-26} W m⁻² Hz⁻¹), the combined Southern Sky Redshift Survey (SSRS2) + Center for Astrophysics-2 (CfA2) survey, and a cluster sample selected from the Automated Plate Measurement (APM) Galaxy Survey (43). We also use the power spectrum resulting from the Lucy inversion of the angular correlation function of the APM galaxy cata-

log (44, 45). The APM galaxy power spectrum is measured in real space, whereas the others are given in redshift space. Each of these power spectra can be scaled by the square of an adjustable bias parameter, which is expected to be near unity for the galaxy surveys (46).

Following the methods of Peacock and Dodds (41), we performed model-dependent corrections for redshift distortions for each galaxy power spectrum (47, 48) and divided by the square of a trial value of the bias factor. We then corrected for nonlinear evolution (49) to produce estimates of the unbiased linear power spectrum from these

galaxy surveys. Comparison with the predicted linear $P(k)$ determined the best-fit bias parameter of each survey for each model (Table 2). We compared the corrected large-scale structure data, the CMB anisotropy observations, and the predicted matter and radiation power spectra and calculated the χ^2 value for each model (Table 3). Only points observed at $k \leq 0.2 h \text{ Mpc}^{-1}$ were used in selecting best-fit bias factors and normalizations and in calculating χ^2 (50). On smaller scales, the linearization process yielded qualitative information despite systematic uncertainties.

Discussion

The current large-scale structure observations agree well with each other in terms of the shape of the uncorrected matter power spectrum (Fig. 2A). The APM clusters are biased compared to galaxies by about a factor of 3, and their power spectrum has a narrower peak and a possible small-scale feature. There is no clear evidence, however, for scale dependence in the bias of the various galaxy surveys on linear scales. The observed galaxy power spectra are smooth, showing no statistically significant oscillations. A peak in the matter power spectrum appears near $k = 0.03 h \text{ Mpc}^{-1}$, which constrains $\Omega_m h$ by identifying the epoch of matter-radiation equality (44). The large-scale structure observations contain too much information to be summarized by a single shape parameter; no value of the traditional CDM shape parameter (51) can simultaneously match the location of this peak and its width.

We find a poor fit for SCDM (Fig. 2B), due to the difference in shape between the theory curve and the data. The best-fit normalization is only 0.91 that of COBE, as the model would otherwise overpredict the σ_8 measurements by an even greater amount. The fit to the CMB is poor, because the Saskatoon (SK) observations (52) would prefer more power. The fit of the data to the TCDM model (Fig. 2C) is better, although the peak of the matter power spectrum is still broader than that found in the data. Agreement with the CMB is harmed by the high normalization versus COBE and the tilt on medium scales.

The best-fit model is CHDM (Fig. 2D). The agreement with the location and shape of the peak of the matter power spectrum is remarkable, with the exception of the APM cluster power spectrum. The agreement with CMB anisotropy detections is excellent. The matter power spectrum of CHDM matches the linearized APM galaxy power spectrum down to nonlinear scales, making this model a good explanation of structure formation far beyond the scales used for our

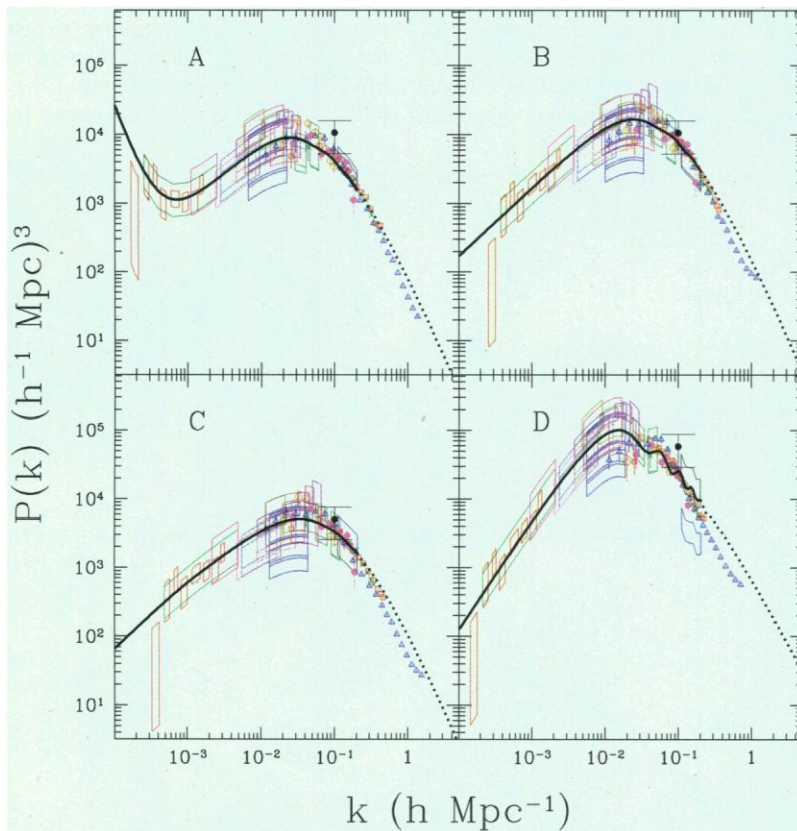


Fig. 3. (A) OCDM, with scale invariance of potential perturbations causing an increase in the matter power spectrum beyond the curvature scale. (B) The Λ CDM model. (C) The ϕ CDM model. (D) The BCDM model.

Table 3. The χ^2 values for our models, computed from data at $k \leq 0.2 h \text{ Mpc}^{-1}$ (60). P is the probability of getting χ^2 greater than or equal to the observed value if a model is correct. df, degrees of freedom.

Model	χ^2_{CMB} (df 34)	$\chi^2_{\sigma_8}$ (df 3)	χ^2_{clus} (df 8)	χ^2_{Cfa} (df 2)	χ^2_{icrs} (df 5)	χ^2_{apm} (df 9)	χ^2_{iras} (df 9)	χ^2_{total} (df 70)	χ^2/df	P
SCDM	46	36	37	0.2	8	121	18	266	3.8	$<10^{-7}$
TCDM	51	5	27	0.4	6	49	11	148	2.1	1.8×10^{-7}
CHDM	30	4	20	3	9	10	11	86	1.2	0.09
OCDM	36	2	24	2	11	42	12	128	1.8	2.9×10^{-5}
Λ CDM	30	3	26	2	12	46	13	132	1.9	1.1×10^{-5}
ϕ CDM	32	4	30	0.1	5	71	12	155	2.2	$<10^{-7}$
BCDM	32	38	33	1	125	225	56	511	7.3	$<10^{-7}$
ICDM	61	3	17	2	21	50	16	170	2.5	$<10^{-7}$
PBH BDM	65	4	22	2	9	30	11	142	2.0	8.3×10^{-7}
Strings + Λ	64	37	20	0.3	8	43	10	182	2.6	$<10^{-7}$

statistical analysis (53).

For the OCDM model (Fig. 3A), $\Omega_m = 0.5$ is favored by the shape of $P(k)$ and the SK and cosmic anisotropy telescope (CAT) (54) CMB anisotropy detections and generates agreement between the two observations of σ_8 . However, the location of the peak of $P(k)$ appears wrong. This model is our second-best fit but is statistically much worse than CHDM. The Λ CDM model (Fig. 3B) is nearly as successful as OCDM. It is a slightly better fit to the CMB but is worse in comparison to large-scale structure. The observations of σ_8 are again in agreement, but the shape of the matter power spectrum does not compare well with that of the APM galaxy survey.

The ϕ CDM model is too broad at the peak and misses a number of APM galaxy data points (Fig. 3C), although its agreement with the other data sets is rather good. It remains to be seen whether other variations of scalar field models can match the observations better. The BCDM model (Fig. 3D) does not fit the data. Choosing parameters to place an acoustic oscillation peak near $k = 0.05 h \text{ Mpc}^{-1}$ has generated the wrong shape for $P(k)$, even though the APM galaxies and clusters seem to fit the first and second oscillations, respectively (55). The main peak of $P(k)$ is in the wrong place; no model with similar oscillations and a baryon content consistent with Big Bang nucleosynthesis can fix that problem (18).

For the ICDM model (Fig. 4A), the fit to the CMB is poor, due to the rise of C_ℓ on COBE scales, too much power in the first peak near $\ell = 100$, and too little power compared to SK. The fit to large-scale structure is mediocre. The PBH BDM model has similar problems compared to the CMB, but the peak location and shape of the matter power spectrum are better (Fig. 4B). The strings + Λ model (Fig. 4C) underestimates the amplitude of the bias-independent measurements and therefore requires a large bias for all types of galaxies, which is difficult to justify.

Conclusions

The rough agreement of CMB anisotropy and large-scale structure observations over a wide range of models suggests that the gravitational instability paradigm of cosmological structure formation is correct. The current set of CMB anisotropy detections may be a poor discriminator among adiabatic models, but it strongly prefers them to non-adiabatic models. Several models (SCDM, TCDM, BCDM, and strings + Λ) have a best-fit normalization significantly different from their COBE normalization and would have been unfairly penalized if normalized

to COBE alone. The strings + Λ model already includes a tensor contribution, but SCDM and BCDM would benefit from adding a gravitational wave component to bring them into better agreement with COBE without changing the amplitude of their scalar perturbations. Adding gravitational waves is not, however, a panacea for those models. In general, the models that are the best fits to the shape of the matter power spectrum prefer to be close to their COBE normalization, which argues against there being a significant tensor contribution to large-angle CMB anisotropies.

Large-scale structure data have more discriminatory power at present than do the CMB anisotropy detections. The average ratio of best-fit biases (b) (Table 2) is $b_{\text{clus}}:b_{\text{cfa}}:b_{\text{lcrs}}:b_{\text{apm}}:b_{\text{irras}} = 3.2:1.3:1.2:1.3:1$ (56). Most models allow optical galaxies to be nearly unbiased tracers of the dark matter distribution. The large-scale structure data are smooth enough to set a limit on the baryon fraction Ω_b/Ω_m ; when that fraction gets higher than 0.1, the fit worsens (57).

By restricting our analysis to the linear regime and correcting for the mildly scale-dependent effects of redshift distortions and nonlinear evolution on those scales, we

made it possible to test models quantitatively. The most likely cosmology is CHDM, which is the only model allowed at the 95% confidence level. The disagreement between the data and the predictions of the other models is sufficient to rule out all of them at above 99% confidence unless there are severe systematic problems in the data (58). CHDM itself is not statistically very likely because of the APM cluster survey $P(k)$, which no model fits much better and which disagrees somewhat with the galaxy power spectra. Dropping the APM cluster $P(k)$ would give CHDM a χ^2 of 66/62, which is within the 68% confidence interval. It is worth investigating whether the APM cluster power spectrum contains a scale-dependent bias or if its errors have somehow been underestimated.

We have extracted the spectrum of primordial density fluctuations from the data and found that it agrees well with that of the CHDM model. This does not provide direct evidence for the existence of HDM, which requires experimental confirmation of neutrino mass. The CHDM model has other observational hurdles to overcome, including evidence for early galaxy formation on small scales where this model has

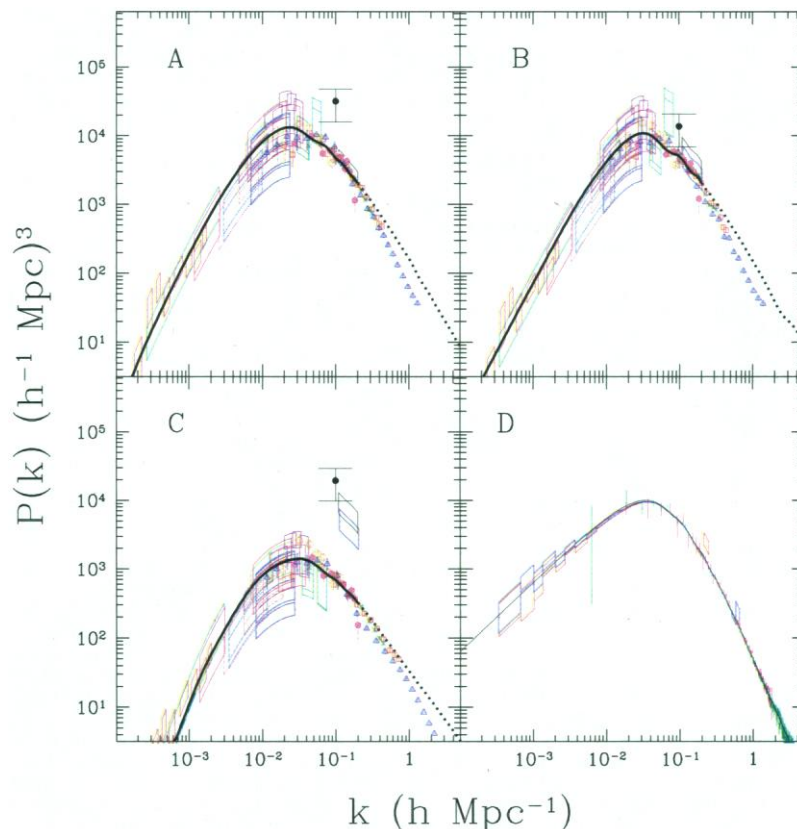


Fig. 4. (A) The ICDM model (66). (B) The PBH BDM model. (C) The strings + Λ model (67). (D) A simulation of high-precision future observations of CMB anisotropy by the MAP (red boxes) and Planck Surveyor (blue boxes) satellites. Green error bars show the accuracy of the SDSS data, and magenta error bars show the accuracy of the 2DF Survey data. The simulated data are indistinguishable from the underlying model (CHDM) for a wide range of k (68).

little power, although it is impressive that CHDM agrees with the linearized APM data out to $k = 1 h \text{ Mpc}^{-1}$. If the rapidly improving Type Ia supernovae observations follow current trends there may be enough statistical power in the direct observations of cosmological parameters to make Λ CDM and Λ CDM preferred to CHDM, although in that case none of these models would be a satisfactory fit to both the supernovae and structure formation observations.

REFERENCES AND NOTES

1. First reported by the COBE DMR team [G. F. Smoot *et al.*, *Astrophys. J.* **396**, L1 (1992)].
2. Less fluctuation growth occurs, for example, in a universe with matter density below the critical Einstein-de Sitter value than in a universe at critical density, because of the weakened role of gravity at late times.
3. D. Scott, J. Silk, M. White, *Science* **268**, 829 (1995).
4. A. N. Taylor and M. Rowan-Robinson, *Nature* **359**, 396 (1992); M. White and D. Scott, *Comments Astrophys* **8**, 289 (1996); S. Dodelson, E. Gates, M. S. Turner, *Science* **274**, 69 (1996); S. Hancock, G. Rocha, A. N. Lasenby, C. M. Gutierrez, *Mon. Not. R. Astron. Soc.* **289**, 505 (1997); J. R. Bond and A. H. Jaffe, in *Proceedings of XXXth Moriond Meeting*, F. R. Bouchet *et al.* Eds. (Editions Frontieres, Gif-Sur-Yvette, France, 1997), pp. 197–208; C. H. Lineweaver and D. Barbosa, *Astrophys. J.* **496**, 624 (1998); M. Webster, M. P. Hobson, A. N. Lasenby, O. Lahav, G. Rocha, <http://xxx.lanl.gov/abs/astro-ph/9802109> [Webster *et al.* include a more detailed analysis of the galaxy distribution of the IRAS redshift survey than is performed here. When we restrict our analysis to the data sets they consider, we find that several models are in good agreement with the data].
5. A. R. Liddle *et al.*, *Mon. Not. R. Astron. Soc.* **278**, 644 (1996); A. R. Liddle, D. H. Lyth, P. T. P. Viana, M. White, *ibid.* **282**, 281 (1996); A. Klypin, J. Primack, J. Holtzman, *Astrophys. J.* **466**, 13 (1996).
6. A. R. Liddle *et al.*, *Mon. Not. R. Astron. Soc.* **281**, 531 (1996).
7. M. White *et al.*, *ibid.* **283**, 107 (1996).
8. Because of theorists' productivity, there are many exotic models we could have used, but we included the most popular variations of Λ CDM and a sampling of promising alternatives.
9. S. Weinberg, *Gravitation and Cosmology* (Wiley, New York, 1972), equations 15.3.11 and 15.3.20; S. Carroll, W. Press, E. Turner, *Annu. Rev. Astron. Astrophys.* **30**, 499 (1992).
10. The primordial power spectrum does not have to be an exact power law; inflationary models predict slight variation of the power-law index with scale. Allowing this spectral index to vary freely makes it more difficult to constrain cosmological models, as shown by E. Gawiser and J. Silk, in *Proceedings, Particle Physics and the Early Universe Conference* (1997), available at <http://www.mrao.cam.ac.uk/ppeuc/proceedings>; E. Gawiser, in *Proceedings of the 18th Texas Symposium on Relativistic Astrophysics*, Chicago, IL, December 1996, A. Olinto, J. Frieman, D. N. Schramm, Eds. (World Scientific, Singapore, in press).
11. E. R. Harrison, *Phys. Rev. D* **1**, 2726 (1970); Ya. B. Zel'dovich, *Mon. Not. R. Astron. Soc.* **160**, 1P (1972); P. J. E. Peebles and J. T. Yu, *Astrophys. J.* **162**, 815 (1970). For the Λ CDM model, we used a primordial power spectrum where the scale invariance of gravitational potential perturbations causes a rise in the matter power spectrum at the curvature scale. Topological defect models with critical matter density have scaling solutions that approximate $n = 1$.
12. E. F. Bunn and M. White, *Astrophys. J.* **480**, 6 (1997).
13. M. Davis *et al.*, *ibid.* **292**, 371 (1985).
14. For the Λ CDM model, see M. White, D. Scott, J. Silk, M. Davis, *Mon. Not. R. Astron. Soc.* **276**, L69 (1995); for the CHDM model, see M. Davis, F. J. Summers, D. Schlegel, *Nature* **359**, 393 (1992); A. Klypin, J. Holtzman, J. Primack, E. Regos, *Astrophys. J.* **416**, 1 (1993); D. Y. Pogosyan and A. A. Starobinsky, *Mon. Not. R. Astron. Soc.* **265**, 507 (1993); E. Choi and D. Ryu, *ibid.*, in press (available at <http://xxx.lanl.gov/abs/astro-ph/9710078>).
15. The neutrino mass is given by $m_\nu = 94 \Omega_\nu h^2 \text{ eV} = 4.7 \text{ eV}$.
16. J. R. Primack, J. Holtzman, A. Klypin, and D. O. Caldwell [*Phys. Rev. Lett.* **74**, 2160 (1995)] suggested a version of CHDM with two equally massive neutrinos to explain the observed cluster abundance, but including the higher value of σ_8 implied by the evolution of the cluster abundance makes a single massive neutrino slightly favored. We find $\Omega_\nu = 0.2$ preferable to $\Omega_\nu = 0.3$ by a small margin. The parameters for CHDM and Λ CDM are within the range found acceptable by (6) and (7).
17. P. G. Ferreira and M. Joyce, *Phys. Rev. Lett.* **79**, 4740 (1998). Several other types of scalar fields have been proposed recently [R. R. Caldwell, R. Dave, P. J. Steinhardt, *ibid.* **80**, 1586 (1998); P. T. P. Viana and A. R. Liddle, *Phys. Rev. D* **57**, 674 (1998); M. S. Turner and M. White, *ibid.* **56**, R4439 (1997); K. Coble, S. Dodelson, J. A. Frieman, *ibid.* **55**, 1851 (1997)]. ϕ CDM is a scalar field model that seems to agree well with the observations.
18. D. J. Eisenstein, W. Hu, J. Silk, A. S. Szalay, *Astrophys. J.* **494**, L1 (1997). To reduce the level of CMB anisotropy that results from its scalar spectral index of $n = 1.6$, Λ CDM has reionization with optical depth to the last scattering surface of $\tau = 0.75$.
19. J. Einasto *et al.*, *Nature* **385**, 139 (1997).
20. S. D. Landy *et al.*, *Astrophys. J.* **456**, L1 (1996).
21. P. J. E. Peebles, *ibid.* **483**, L1 (1997).
22. <http://xxx.lanl.gov/abs/astro-ph/9805212>.
23. The numerous atomic hydrogen clouds seen at red shifts $z \sim 3$ by their absorption of quasar emission are referred to as the Lyman α forest. They may represent the early stages of galaxy formation.
24. N. Sugiyama and J. Silk, in preparation.
25. C. Alcock *et al.*, *Astrophys. J.* **486**, 697 (1997).
26. A. D. Albrecht, R. A. Battye, J. Robinson, *Phys. Rev. Lett.* **79**, 4736 (1997). Topological defects are active sources that originate in a symmetry breaking in the early universe and seed primordial density perturbations. Their predictions for matter and radiation fluctuations are similar to inflationary models, although the matter distribution is expected to be non-Gaussian.
27. R. A. Battye, J. Robinson, A. Albrecht, *Phys. Rev. Lett.*, in preparation (available at <http://xxx.lanl.gov/abs/astro-ph/9711336>); see also P. P. Avelino, R. R. Caldwell, C. J. A. P. Martins, *Phys. Rev. D* **56**, 4568 (1997).
28. U. Seljak and M. Zaldarriaga, *Astrophys. J.* **469**, 437 (1996); M. Zaldarriaga, U. Seljak, E. Bertschinger, *ibid.* **494**, 491 (1998).
29. D. Tytler *et al.*, *Nature* **381**, 207 (1996).
30. D. Branch, *Annu. Rev. Astron. Astrophys.*, in preparation (available at <http://xxx.lanl.gov/abs/astro-ph/9801065>); W. L. Freedman, in *Critical Dialogues in Cosmology*, N. Turok, Ed. (World Scientific, Singapore, 1997), pp. 92–129; A. Sandage and G. A. Tammann, in *ibid.*, pp. 130–155.
31. B. Chaboyer, P. Demarque, P. J. Kernan, L. M. Krauss, *Astrophys. J.* **494**, 96 (1998).
32. J. P. Gardner, N. Katz, D. H. Weinberg, L. Hernquist, *ibid.* **486**, 42 (1997); C. P. Ma, E. Bertschinger, L. Hernquist, D. H. Weinberg, N. Katz, *ibid.* **484**, L1 (1997). The improved hydrodynamic simulations of M. G. Haehnelt, M. Steinmetz, and M. Rauch (<http://xxx.lanl.gov/abs/astro-ph/9706201>) indicate, however, that all typical structure formation models have enough small-scale power to produce the observations of high-redshift damped Lyman α systems.
33. M. Bartelmann, A. Huss, J. M. Colberg, A. Jenkins, F. R. Pearce, *Astron. Astrophys.* **330**, 1 (1998).
34. A. E. Evrard, *Mon. Not. R. Astron. Soc.* **292**, 289 (1997).
35. S. Perlmutter *et al.*, *Bull. Am. Astron. Soc.* **29**, 1351 (1997); P. M. Garnavich *et al.*, *Astrophys. J.* **493**, L53 (1997); S. Perlmutter *et al.*, *Nature* **391**, 51 (1997).
36. C. S. Kochanek, *Astrophys. J.* **466**, 638 (1996).
37. C. L. Bennett *et al.*, *ibid.* **464**, L1 (1996); J. C. Mather *et al.*, *ibid.* **420**, 439 (1994). This is based on the standard definition for a "flat" power spectrum, $dT = [\ell(\ell + 1)C_\ell/2\pi]^{1/2} T_{\text{CMB}}$.
38. Because of projection effects, fluctuations at the last scattering surface on a given angular scale are generated by density perturbations from a range of spatial scales centered on a wavenumber k (given in units of h per megaparsec), where $\ell = k\eta_0$ for a coordinate distance to the last scattering surface given by $\eta_0 = 2cH_0^{-1} \Omega_m^{-\alpha}$; $\alpha = 0.4$ in a flat universe and $\alpha = 1$ in an open universe [N. Vittorio and J. Silk, *ibid.* **385**, L9 (1992)].
39. P. T. P. Viana and A. R. Liddle, *Mon. Not. R. Astron. Soc.* **281**, 323 (1996).
40. N. A. Bahcall, X. Fan, R. Cen, *Astrophys. J.* **485**, L53 (1997); X. Fan, N. A. Bahcall, R. Cen, *ibid.* **490**, L123 (1997). Much attention has recently been paid to using the abundance of galaxy clusters at $z = 0.2$ to 0.5 as a probe of Ω_m , [for example, R. G. Carlberg, S. L. Morris, H. K. C. Yee, E. Ellingson, *ibid.* **479**, 82 (1997)]. We accounted for this constraint by using both the value of σ_8 derived from the $z = 0$ cluster abundance and that preferred by the evolution of the cluster abundance; in models with the preferred value of Ω_m , these two observations of σ_8 will agree. We used the method of W. A. Chiu, J. P. Ostriker, and M. A. Strauss [*ibid.* **494**, 479 (1998)] to interpret the observed cluster abundances and their evolution as measurements of σ_8 for the non-Gaussian strings + Λ model. For Λ CDM, we used a single determination of $\sigma_8 = 0.9 \pm 0.1$ (22).
41. J. A. Peacock and S. J. Dodds, *Mon. Not. R. Astron. Soc.* **267**, 1020 (1994).
42. T. Kolatt and A. Dekel, *Astrophys. J.* **479**, 592 (1997). We used only the measurement at $k = 0.1 h \text{ Mpc}^{-1}$, which is confirmed by the likelihood analysis of S. Zaroubi, I. Zehavi, A. Dekel, Y. Hoffman, and T. Kolatt [*ibid.* **486**, 21 (1997)]. A full discussion of peculiar velocity data is given by M. Gramann [*ibid.* **493**, 28 (1998)].
43. The four surveys are described, respectively, in the following sources: H. Lin *et al.*, *ibid.* **471**, 617 (1996); H. Tadros and G. Efsthathiou, *Mon. Not. R. Astron. Soc.* **276**, L45 (1995); L. N. Da Costa *et al.*, *Astrophys. J.* **437**, L1 (1994); H. Tadros, G. Efsthathiou, G. Dalton, in preparation (available at <http://xxx.lanl.gov/abs/astro-ph/9708259>). We used the APM cluster $P(k)$ only for $k \leq 0.12 h \text{ Mpc}^{-1}$ to avoid possible artifacts of the survey window function at higher k . The APM cluster $P(k)$ was analyzed for several background cosmologies, and we used the version most appropriate to each model. We chose the $101 h^{-1} \text{ Mpc}$ version of the SSRS2+CfA2 survey to avoid the luminosity bias present in the deeper sample noted by C. Park, M. S. Vogeley, M. J. Geller, and J. P. Huchra [*Astrophys. J.* **431**, 569 (1994)].
44. E. Gaztañaga and C. M. Baugh, *Mon. Not. R. Astron. Soc.* **294**, 229 (1998). We dropped the first four reported APM points because they appear to be artifacts of the data analysis.
45. C. M. Baugh and G. Efsthathiou, *ibid.* **265**, 145 (1993).
46. Galaxies may be more or less common than 1σ peaks of the dark matter distribution, so they are biased tracers of the mass. Each morphological type is expected to have a slightly different scale-independent bias. Clusters have a large bias because they trace high-density peaks of the primordial density distribution, and such peaks are themselves highly clustered [see N. Kaiser, *Astrophys. J.* **284**, L9 (1984)]. Our assumption that bias is scale-independent is supported by the following: G. Kauffmann, A. Nusser, M. Steinmetz, *Mon. Not. R. Astron. Soc.* **286**, 795 (1997); R. G. Mann, J. A. Peacock, A. F. Heavens, *ibid.* **293**, 209 (1998); R. J. Scherrer and D. H. Weinberg, <http://xxx.lanl.gov/abs/astro-ph/9712192>. Peculiar velocities arise because of the gravity of the underlying dark matter, so they produce a bias-independent measurement of the matter power spectrum. Both observations of σ_8 are also bias-independent.
47. The power spectrum observed in redshift space is related to that in real space by $P_r(k) = (1 + \beta\mu^2)^2 D(k\mu_\sigma) P_{\text{real}}(k)$, where the first term gives the

Kaiser distortion [N. Kaiser, *Mon. Not. R. Astr. Soc.* **227**, 1 (1987)] from coherent infall of galaxies with bias b as a function of $\beta = \Omega_m^{0.6} b$, and the second term is the damping of such distortions by the root-mean-square pairwise galaxy velocity dispersion (σ_p), measured in units of H_0 . This velocity dispersion leads to the so-called fingers-of-God effect in redshift surveys. For an exponential velocity distribution, $D(k, \mu, \sigma_p) = [1 + (k\mu\sigma_p)^2/2]^{-1}$. We averaged over μ , the cosine of the angle between the line of sight and a given wave vector \mathbf{k} , to produce an estimate of the real-space power spectrum $P_{\text{real}}(k) = P_g(k)/f(k, b)$. Defining $K = k\sigma_p/\sqrt{2}$, this gave [W. E. Ballinger, thesis, University of Edinburgh (1997)]:

$$f(k, b) = \frac{1}{K} \left[\tan^{-1}(K) \left(1 - \frac{2\beta}{K^2} + \frac{\beta^2}{K^4} \right) + \frac{2\beta}{K} + \frac{\beta^2}{3K} - \frac{\beta^2}{K^3} \right] \quad (3)$$

For the pairwise velocity dispersion, we used the observation from S. D. Landy, A. S. Szalay, and T. J. Broadhurst [*Astrophys. J.* **494**, L133 (1998)] of $\sigma_p = 3.63 h^{-1}$ Mpc. Their determination that the velocity distribution is exponential was the motivation for using that form for the damping term. We tried using the higher value of $\sigma_p = 5.70 h^{-1}$ Mpc (Y. P. Jing, H. J. Mo, G. Börner, *ibid.*, p. 1), and it made only a small difference on quasilinear scales; at $k = 0.2 h$ Mpc $^{-1}$ the scale dependence of the redshift distortions is a 15% effect for the value of $3.63 h^{-1}$ Mpc and twice that for the higher one. This systematic uncertainty in the pairwise velocity dispersion makes the corrected real-space power spectrum somewhat unreliable on smaller scales. For the cluster power spectrum, we used only the scale-independent Kaiser distortion term to correct for redshift distortions as the clusters are engaged in coherent infall onto superclusters. The APM galaxy power spectrum was corrected for bias only, as it does not have redshift distortions.

18. C. Smith, A. Klypin, M. Gross, J. Primack, and J. Holtzman (in preparation; available at <http://xxx.lanl.gov/abs/astro-ph/9702099>) give a full discussion of the effects of varying σ_p and propagating this systematic uncertainty through the linearization procedure; their results confirm that the systematic uncertainty is small up to $k = 0.2 h$ Mpc $^{-1}$.
19. Because collapsing structure leads to a change of physical scale, the observed nonlinear scales (k_{nl}) can be corrected to their linear values, given by $k_l = (1 + \Delta_{\text{nl}}^2)^{-1/3} k_{\text{nl}}$, where $\Delta^2 = k^2 P(k)/2\pi^2$. The nonlinear evolution is given by $\Delta_{\text{nl}}^2 = f(\Delta^2)$. A semianalytic fit for this function, with 10% accuracy compared to that of numerical simulations, is given by J. A. Peacock and S. J. Dodds [*Mon. Not. R. Astron. Soc.* **280**, L19 (1996)]. The accuracy of this formula is confirmed in (48). This correction is model-dependent, as it assumes a local slope for the original linear power spectrum based on the model being tested. By inverting the formula numerically, we linearized the unbiased real-space $P(k)$. Nonlinear evolution is significant only at $k \geq 0.2 h$ Mpc $^{-1}$. At smaller k , the linearization preserves the shape of the observed nonlinear $P(k)$ while sliding the data points to smaller k ; its main effect is to shrink the error bars slightly.
20. We have rebinned some of the galaxy survey data to make the points independent. Our conclusions are unaffected by varying the nonlinear cutoff between $k = 0.15 h$ Mpc $^{-1}$ and $k = 0.25 h$ Mpc $^{-1}$.
21. Defined by G. Efstathiou, J. R. Bond, and S. D. M. White [*Mon. Not. R. Astron. Soc.* **258**, 1P (1992)].
22. C. B. Netterfield *et al.*, *Astrophys. J.* **474**, 47 (1997).

We used the recalibration of SK from E. Leitch [thesis, California Institute of Technology (1997)].

53. J. A. Peacock, *Mon. Not. R. Astron. Soc.* **284**, 885 (1997) and (48) also found good agreement between the linearized observations and linear theory under the CHDM model.
54. P. F. S. Scott *et al.*, *Astrophys. J.* **461**, L1 (1996); J. C. Baker, in *Proceedings, Particle Physics and the Early Universe Conference* (1997), available at <http://www.mrao.cam.ac.uk/ppauc/proceedings>.
55. We averaged the predictions of the matter power spectrum over the window function of the observations to take into account the possible smoothing of these oscillations during observation. To make the linearization procedure work smoothly, we fixed the local slope of the linear power spectrum.
56. This is roughly consistent with the bias ratios found by (41).
57. See D. M. Goldberg and M. A. Strauss, *Astrophys. J.* **495**, 29 (1998) for the future prospects of this constraint.
58. If the APM Galaxy $P(k)$ were ignored, Λ CDM, Λ CDM, and ϕ CDM would become much better fits but would still be ruled out at the 95% confidence level.
59. The ϕ CDM model has a scalar field energy density of $\Omega_\phi = 0.08$. The PBH BDM model has 30% of critical density in primordial black holes, which act like CDM but actually contain baryonic matter.
60. The χ^2_{res} category includes the contribution from peculiar velocity measurements. The degree of freedom used by normalizing is counted under χ^2_{CMB} , and each galaxy survey loses one degree of freedom in choosing a best-fit bias. The Λ CDM model has one less degree of freedom in the χ^2_{res} column and a total of 69 degrees of freedom.
61. The error bars include uncertainties due to instrument noise, calibration uncertainty, sample variance from observing only part of the sky, and cosmic variance from observing at only one location in the universe. The calibration errors were added in quadrature. Although calibration errors are correlated for multiple observations by the same instrument, they have been treated as independent, which is a good approximation after the recalibration of SK by Leitch (52).
62. CMB anisotropy observations are compiled by G. F. Smoot and D. Scott, *Rev. Part. Prop.*, [on-line] (available at <http://xxx.lanl.gov/abs/astro-ph/9711069>) and at <http://www.sns.ias.edu/~max/cmb/experiments.html>. Shown here are observations from COBE (M. Tegmark and A. Hamilton, <http://xxx.lanl.gov/abs/astro-ph/9702019>), FIRS [K. Ganga, L. Page, E. Cheng., S. Meyers, *Astrophys. J.* **432**, L15 (1993)], Tenerife [C. M. Gutierrez *et al.*, *ibid.* **480**, L83 (1997)], the South Pole [J. O. Gundersen *et al.*, *ibid.* **443**, L57, (1994)], BAM [G. S. Tucker *et al.*, *ibid.* **475**, L74 (1997)], ARGO [S. Masi *et al.*, *ibid.* **463**, L47 (1996)], Python [S. R. Platt *et al.*, *ibid.* **475**, L1 (1997)], MAX (Microwave Anisotropy Experiment) [M. Lim *et al.*, *ibid.* **469**, L69 (1996); S. T. Tanaka *et al.*, *ibid.* **468**, L81 (1996)], MSAM (Medium-Scale Anisotropy Measurement) [E. S. Cheng *et al.*, *ibid.* **488**, L59 (1997)], SK (52), and CAT (54).
63. The width of the box represents the range of spatial scales to which σ_8 is sensitive, and the height shows the 68% confidence interval. The half-max window for σ_8 is from $k = 0.05$ to $k = 0.3$, but it has been narrowed for clarity. The width of the window function of the peculiar velocity observation is shown by the ends of its error bars, which include cosmic variance. This observation scales as $\Omega_m^{-1.2}$ (the square of the growing mode). The determination of $P(k)$ from the value of σ_8 implied by the $z = 0$ cluster abun-

dance scales roughly as Ω_m^{-1} due to the relationship between the observed mass and the pre-collapse radius of rich clusters. The observation of σ_8 from the evolution of the cluster abundance is nearly independent of Ω_m .

64. The high- k end of the LCRS data shows that the combination of deconvolving the fingers-of-God effect and linearizing the data has kept the shape the same but moved the points along that curve and reduced the error bars. The linearization of the APM dataset has removed the inflection at $k = 0.2 h$ Mpc $^{-1}$.
65. Each model has a particular value of η_0 ; varying η_0 moves the entire set of boxes horizontally. Comparison of the CMB anisotropy predictions of each model with observations gives the vertical placement of each box, showing the inferred amplitude of matter density fluctuations at that scale. The boxes for CMB anisotropy detections and σ_8 follow the local shape of each model's $P(k)$ to indicate they are a model-dependent averaging of the power over a range of k .
66. The strong rise of the matter power spectrum is caused by the sharp tilt of the model away from scale invariance. The linearization procedure used was calibrated for Gaussian models, but nonlinear evolution is expected to be similar under the χ^2 distribution [A. Stirling, thesis, University of Edinburgh (1998)].
67. It is possible that the linearization procedure needs to be adjusted to account for non-Gaussianity in the matter distribution, but the reduced power of this model weakens the effects of nonlinear evolution.
68. Microwave anisotropy probe (MAP) and Planck parameters were taken from J. R. Bond, G. Efstathiou, and M. Tegmark [*Mon. Not. R. Astron. Soc.* **291**, L33 (1997)]. The Sloan Digital Sky Survey (SDSS) data are from M. Vogeley (personal communication), and the 2-Degree Field (2DF) Survey data are from S. Cole, S. Hatton, D. Weinberg, C. S. Frenk, <http://xxx.lanl.gov/abs/astro-ph/9801250>. No attempt has been made in Fig. 4D to account for redshift distortions or nonlinear evolution. The overlap in scale between CMB anisotropy detections and large-scale structure observations should increase tremendously in the next several years, and the errors in these measurements should decrease significantly. W. Hu, D. J. Eisenstein, and M. Tegmark (in preparation; available at <http://xxx.lanl.gov/abs/astro-ph/9712057>) examine how well Ω_v can be determined by SDSS observations, and Y. Wang, D. N. Spergel, and M. A. Strauss (in preparation; available at <http://xxx.lanl.gov/abs/astro-ph/9802231>) discuss the ability of combined MAP and SDSS observations to constrain cosmological parameters.
69. We gratefully acknowledge the contributions of U. Seljak and M. Zaldarriaga (CMBFAST), P. Ferreira (ϕ CDM), J. Peebles (Λ CDM), N. Sugiyama (PBH BDM), J. Robinson (strings + Λ), H. Tadros (APM cluster analysis for various cosmologies), and the efforts of hundreds of observers who gathered the data. This work benefited from conversations with H. Tadros, M. White, M. Vogeley, P. Viana, A. Taylor, A. Stirling, J. Robinson, J. Peebles, J. Peacock, A. Liddle, A. Jaffe, W. Hu, A. Heavens, G. Evrard, C. Baugh, and W. Ballinger. We thank L. Moustakas for comments on a draft of this paper. E.G. acknowledges the support of an NSF Graduate Fellowship. We thank the Institut d'Astrophysique de Paris for hospitality during the completion of this research. Our data compilation and full-size figures are available at <http://cfpa.berkeley.edu/home.html>.

5 December 1997; accepted 8 April 1998